Dielectric Modulation of Two-Dimensional Dipolar Materials

Ziwei Wang and Erik Luijten

Dielectric modulation of two-dimensional dipolar materials

Ziwei Wang[1] and Erik Luijten[1, 2, *]

[1] *Graduate Program in Applied Physics, Northwestern University, Evanston, Illinois 60208, U.S.A.*
[2] *Departments of Materials Science & Engineering,*
Engineering Sciences & Applied Mathematics, and Physics & Astronomy,
Northwestern University, Evanston, Illinois 60208, U.S.A.

(Dated: June 10, 2019)

Spontaneous pattern formation plays an important role in a wide variety of natural phenomena and materials systems. A key ingredient for the occurrence of modulated phases is the presence of competing interactions, generally of different physical origins. We demonstrate that in dipolar films, a prototypical system for pattern formation, patterns can be induced by dielectric effects alone. A rich phase diagram arises, where striped and circular morphologies emerge with geometric properties that can be controlled through variation of particle shape and substrate permittivity or permeability. These effects are particularly enhanced by metamaterial substrates.

Spontaneous pattern formation and modulation of phases in two dimensions occur in a diverse set of physical, chemical, and biological systems [1, 2]. The domains can exhibit a variety of patterns—notably stripes, islands, and circular droplets—that are often characterized by spatial periodicity. Examples include the orientational patterns in ferromagnetic thin films [3–5], the domain structure of dipolar Langmuir monolayers [6, 7], and microphase separation in block copolymer melts [8, 9]. These phenomena have significant potential for technological applications, such as nanofabrication [10, 11] and nanomagnetism [12].

One of the central common, and in fact necessary, factors underlying pattern formation in thermodynamic equilibrium is the presence of competing interactions [1, 2]. Dipolar interactions, so ubiquitous in nature, have emerged as the most basic and widely studied starting point. Yet, a second potential is required for modulated patterns to appear, such as the short-range exchange interaction [4, 13, 14], interfacial energy [6, 7], geometric constraints [15–17], or an external field [18, 19]. No modulated phases have been reported in systems with solely dipolar interactions.

Two-dimensional (2D) dipolar systems exhibit a rich phase diagram [20–24], with an isotropic–polymeric phase transition at low surface densities [21, 24] and more complicated structures as well as orientational ordering at high densities [20, 22]. Although these systems have received widespread attention, a parameter that has been mostly ignored (with dipolar particles confined between metallic plates as a notable exception [25, 26]) is the dielectric mismatch between the substrate and the medium containing the dipolar particles. This omission is noteworthy, given the demonstrated effect of substrate permittivity on properties of a wide range of electromagnetic systems, from plasmonics [27] to ion mobilities in electrolytes [28]. Moreover, with the emergence of electromagnetic metamaterials [29, 30], in which the electric permittivity and/or magnetic permeability are negative, the magnitude of polarization effects can be greatly enhanced [31, 32].

Here, we demonstrate that variation of dielectric mismatch can qualitatively alter the orientational phases of (quasi-)2D dipolar systems. Remarkably, even *modulated* phases can be induced in purely dipolar systems, without the need for external fields or other interactions. We elucidate the origin of the different phases and map the corresponding phase diagram. In addition, we illustrate how even within an individual phase the characteristic length scale can be accurately controlled. Throughout this work, we employ electric dipoles, yet all our findings are directly applicable to magnetic dipolar systems as well [33]. There, tuning of the interfacial dielectric contrast must be replaced by variation of the permeability of the substrate. Experimental realizations of the model studied here include charged Janus colloids [34] and ferromagnetic particles. Various aspects of this work pertain to metamaterial substrates with negative *static* permittivity or permeability. Whereas the former can be realized in a wide range of materials (e.g., metals [35, 36], quasi-2D crystals [37], and nanoparticle [38, 39] and polymeric systems [40]), the latter can be realized by including active components in artificial metamaterials [41].

We examine monolayers of $N = N_x \times N_y$ spheres of diameter d that each carry a point dipole $\boldsymbol{\mu}$. To minimize the influence of the underlying lattice [14], the particles are placed on a hexagonal lattice with lattice constant a and dimensions $L_x = N_x a$, $L_y = \sqrt{3} N_y a / 2$, periodically replicated in the x and y directions. All particles have fixed z-coordinate $d/2$ and are embedded in a medium with uniform permittivity ε_{m}. The substrate has permittivity ε_{s}, so that there is a dielectric mismatch at $z = 0$. We study this system via Monte Carlo simulations in the canonical ensemble where only 3D rotations of the dipoles are permitted. Owing to the piecewise uniform permittivity, the electric dipoles induce surface polarization charge at the substrate interface. Mathematically, the influence of this polarization is most conveniently phrased in terms of "image" dipoles, centered at $z = -d/2$ and with dipole moment $\boldsymbol{\mu}'$ (Fig. 1).
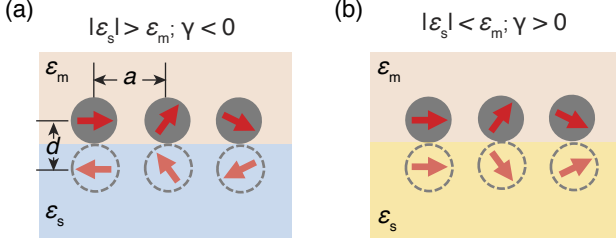
FIG. 1. Schematic depiction of a system of 2D hexagonally packed dipolar spheres immersed in a uniform dielectric medium with permittivity ε_{m} above of a dielectric substrate with permittivity ε_{s}. To account for the polarization charges induced at the interface, we employ "image" dipoles (dashed circles). (a) For high-permittivity substrates (as well as for metamaterials with sufficiently negative permittivity), the in-plane component of these induced dipoles is anti-parallel to their counterpart above the surface, whereas the perpendicular component is parallel. (b) For substrate materials with small absolute permittivity, the situation is reversed. In both cases, nonintuitive collective behavior can emerge, since the images are induced by individual dipoles, but interact with all other dipoles above the substrates.

The Hamiltonian of the system is characterized by two energy scales, the interaction between neighboring dipoles $\lambda_{\mathrm{dd}} = \mu^2/(\varepsilon_{\mathrm{m}} a^3 k_{\mathrm{B}} T)$ and the dipole–image coupling $\lambda_{\mathrm{di}} = \gamma \mu^2/(\varepsilon_{\mathrm{m}} d^3 k_{\mathrm{B}} T) = \gamma \lambda_{\mathrm{dd}}/\alpha^3$, where $\gamma = (\varepsilon_{\mathrm{m}} - \varepsilon_{\mathrm{s}})/(\varepsilon_{\mathrm{m}} + \varepsilon_{\mathrm{s}})$ is the dielectric mismatch, $\alpha = d/a$ is reduced by the lattice constant a, $\mu = |\boldsymbol{\mu}|$, k_{B} is Boltzmann's constant, and T the temperature. We choose a as the unit length and use a tilde to denote reduced lengths. The Hamiltonian reads

$$\frac{\mathcal{H}}{k_{\mathrm{B}} T} = \frac{1}{2} \sum_{i=1}^{N} \sum_{\mathbf{n}}^{\infty} \left\{ \lambda_{\mathrm{dd}} \sum_{j=1}^{N} {}' \frac{\hat{\boldsymbol{\mu}}_i \cdot \hat{\boldsymbol{\mu}}_j - 3(\hat{\boldsymbol{\mu}}_i \cdot \hat{\mathbf{r}}_{ij}^{\mathrm{rep}})(\hat{\boldsymbol{\mu}}_j \cdot \hat{\mathbf{r}}_{ij}^{\mathrm{rep}})}{|\tilde{\mathbf{r}}_{ij}^{\mathrm{rep}}|^3} \right.$$
$$\left. + \lambda_{\mathrm{di}} \sum_{j=1}^{N} \frac{\hat{\boldsymbol{\mu}}_i \cdot \hat{\boldsymbol{\mu}}'_j - 3(\hat{\boldsymbol{\mu}}_i \cdot \hat{\mathbf{r}}_{ij}'^{\mathrm{rep}})(\hat{\boldsymbol{\mu}}'_j \cdot \hat{\mathbf{r}}_{ij}'^{\mathrm{rep}})}{\left|1 + |\tilde{\mathbf{r}}_{ij}^{\mathrm{rep}}/\alpha|^2\right|^{3/2}} \right\} ,$$

where $\hat{\boldsymbol{\mu}}_i = \boldsymbol{\mu}_i/\mu$ and $\hat{\boldsymbol{\mu}}'_i = (\mu_{i,x}, \mu_{i,y}, -\mu_{i,z})/\mu$. The periodicity of the lattice is accounted for via summation over $\mathbf{n} = (n_x, n_y, 0)$ $(n_x, n_y \in \mathbb{Z})$, where the prime indicates that $i \neq j$ for $\mathbf{n} = \mathbf{0}$. The vector $\tilde{\mathbf{r}}_{ij}^{\mathrm{rep}} = (\tilde{r}_{j,x} - \tilde{r}_{i,x} + n_x \tilde{L}_x, \tilde{r}_{j,y} - \tilde{r}_{i,y} + n_y \tilde{L}_y, 0)$ points from dipole i to (a replica of) dipole j, with corresponding unit vector $\hat{\mathbf{r}}_{ij}^{\mathrm{rep}}$, and $\tilde{\mathbf{r}}_{ij}'^{\mathrm{rep}} = (\tilde{r}_{j,x} - \tilde{r}_{i,x} + n_x \tilde{L}_x, \tilde{r}_{j,y} - \tilde{r}_{i,y} + n_y \tilde{L}_y, -\alpha)$ points from dipole i to (a replica of) image dipole j, with corresponding unit vector $\hat{\mathbf{r}}_{ij}'^{\mathrm{rep}}$. Whereas λ_{dd} and λ_{di} control the total contributions of the dipole–dipole (D–D) and dipole–image (D–I) interactions to the system energy, respectively, the geometric factor α determines the ratio between the second-order (and higher) contributions to the D–I interaction (i.e., between dipoles and images of other dipoles) and the first-order D–I interaction (between dipoles and their own images), which only

depends on λ_{di} (which we regard as independent of α as it can be controlled via γ). The observation that α can serve as an independent control parameter has profound consequences for the tunability of patterns that arise for different choices of the coupling strength and dielectric mismatch, as we will explore below.

In practice, we compute the energy via 3D dipolar Ewald summation (relative precision 10^{-5}) modified to include image charges and supplemented with a slab correction [42]. For each parameter choice, we employ 5×10^5 Monte Carlo cycles of N rotational moves.

To quantify the global orientational order, we introduce the parameters P_1 and P_2 [43]. For an instantaneous configuration, P_2 is the largest eigenvalue of the ordering matrix $Q = \frac{1}{2N} \sum_{i=1}^{N} (3 \hat{\boldsymbol{\mu}}_i \hat{\boldsymbol{\mu}}_i - I)$, where I is the identity matrix. The corresponding normalized eigenvector is the global director $\hat{\boldsymbol{d}}$ from which the instantaneous value of P_1 follows as $P_1 = \frac{1}{N} |\sum_{i=1}^{N} \hat{\boldsymbol{\mu}}_i \cdot \hat{\boldsymbol{d}}|$. Whereas P_2 merely characterizes global alignment (nematic order) of the dipolar particles, P_1 is a measure of the global polarization. The degree of *uniaxial* alignment (along the z axis) is quantified by $Q_{zz} = \langle \frac{1}{2N} \sum_{i=1}^{N} (3 \hat{\mu}_{i,z}^2 - 1) \rangle$, where Q_{zz} vanishes in orientationally isotropic states, whereas $Q_{zz} = -0.5$ and $Q_{zz} = 1$ reflect configurations of perfectly in-plane or out-of-plane dipoles, respectively.

To establish a baseline, we examine a system of dense-packed spheres ($\alpha = 1$) in the absence of dielectric contrast at the interface ($\gamma = 0$). In this case, the energy is minimized by head-to-tail chains, yielding an in-plane ferroelectric (IF) state at strong couplings (Fig. 2a) [20, 21]. Note that this is indeed a *global*, long-range ferroelectric order, unlike the vortex-like structure observed for quasi-2D dipolar spheres with positions that are not constrained to a lattice structure [21]. This tendency of dipolar interactions to favor arrangements with in-plane orientation is enhanced in the presence of low-permittivity substrates ($\gamma > 0$), since the interaction energy of dipoles with the induced surface charge is also minimized for such configurations. More interesting is the situation of substrates with a higher permittivity than the medium ($\gamma < 0$), where this energy is minimized for *perpendicular* dipoles. The resulting competition between the dipole–dipole interactions favoring in-plane ferroelectric ordering and the dipole–polarization interaction favoring out-of-plane configurations raises the possibility of a dielectrically induced structural transition.

The magnitude of polarization effects, especially the first-order D–I interaction, is controlled by λ_{di}. This corresponds to the surface anisotropy in magnetic films [15], which promotes the out-of-plane orientation of dipoles. λ_{di} can be varied by either the dielectric mismatch at the interface γ or the geometric ratio α. Decreasing the latter from $\alpha = 1$ to $\alpha = \frac{2}{3}$ while keeping $\lambda_{\mathrm{dd}} = 5$ leads to $\lambda_{\mathrm{di}} = -16.875$ for a perfectly conducting substrate ($\gamma = -1$). As shown in Fig. 2b, this indeed transforms
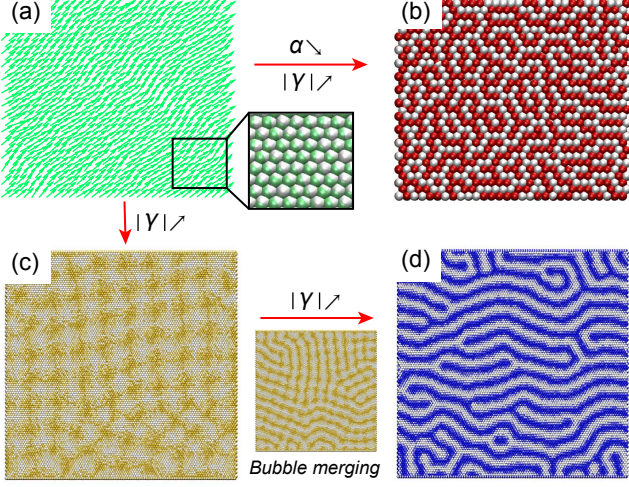
FIG. 2. Typical structures formed by $N = 100 \times 114$ dipolar spheres placed on a 2D hexagonal lattice at dipolar coupling $\lambda_{dd} = 5$. (a) Representative partial (30×30) configuration in the absence of dielectric contrast ($\varepsilon_s = \varepsilon_m$, so $\gamma = 0$ and $\lambda_{di} = 0$) and at packing $\alpha = 1$, showing an IF phase with $P_1 = 0.88$, $P_2 = 0.68$, $Q_{zz} = -0.43$. (b) Same subsample on a perfectly conducting substrate ($\varepsilon_s = +\infty$, $\gamma = -1$) with geometric ratio $\alpha = \frac{2}{3}$, so that the dipole–image coupling is raised to $\lambda_{di} = -16.875$. This results in an OAF phase with $P_1 = 0.01$, $P_2 = 0.79$, $Q_{zz} = 0.78$. (c) Snapshot of the full dense-packed ($\alpha = 1$) system on a metamaterial substrate with $\gamma = -1.6$, exhibiting a bubble phase with $P_1 = 0.01$, $P_2 = 0.23$, $Q_{zz} = -0.12$. (d) As the dielectric contrast is increased further to $\gamma = -3$, the bubble phase transforms to a stripe-like phase with $P_1 = 0.01$, $P_2 = 0.34$, $Q_{zz} = 0.12$. Between the bubble and stripe phases, the bubbles gradually merge into stripes, see snapshot between panels (c) and (d), for $\gamma = -2$. Colors characterize the different phases: IF phase – green; OAF phase – red; bubble phase – yellow; stripe phase – blue.

the IF state into a state with out-of-plane orientation. Owing to the strong interaction of the dipoles with their own images, they are predominantly aligned with the z-axis, so that P_2 and Q_{zz} are close to 1. Simultaneously, the nearest-neighbor dipolar interaction is minimized by an antiparallel arrangement, i.e., an out-of-plane antiferroelectric (OAF) state with $P_1 \approx 0$. This structure is confirmed by the orientational pair correlation function (not shown). Experimentally, α can be reduced by increasing the lattice constant either through variation of the particle shape or by employing a patterned substrate to control the lattice structure [44]. Alternatively, polarization effects can be enhanced (at fixed λ_{dd}) by increasing the magnitude of dielectric mismatch γ. Although $|\gamma|$ is bounded by 1 for conventional materials (i.e., the magnitude of an image dipole cannot exceed the real dipole), this constraint is lifted for a negative-permittivity material (or negative-permeability material for magnetic dipoles) [31, 32]. Specifically, $\gamma < -1$ when $\varepsilon_s < -\varepsilon_m$. Remarkably, this additional control
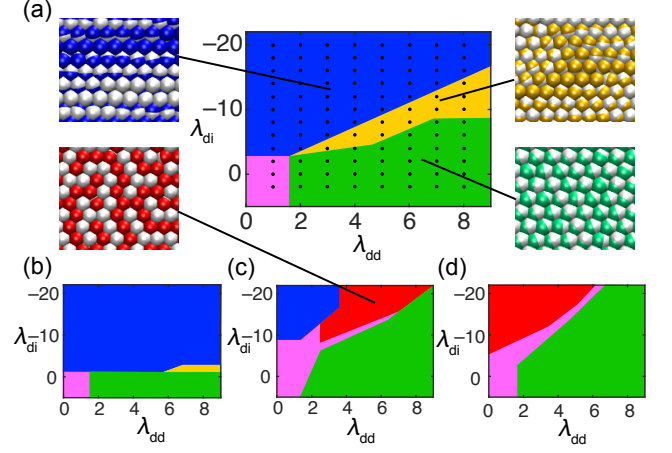

FIG. 3. Phase diagrams parametrized by λ_{dd} and λ_{di}, at different values of the geometric factor α: (a) $\alpha = 1$; (b) $\alpha = 3$; (c) $\alpha = \frac{2}{3}$; (d) $\alpha = \frac{1}{3}$. Colors characterize the different phases: IF phase – green; OAF phase – red; bubble phase – yellow; stripe phase – blue; disordered phase – pink. Phase boundaries are drawn based on discrete simulation data points with positions indicated by black dots in (a).

parameter gives rise to new modulated phases. At fixed $\alpha = 1$ and $\lambda_{dd} = 5$, increasing the dielectric contrast to $\gamma = -1.6$ ($\lambda_{di} = -8$) yields the "bubble" phase (Fig. 2c), followed by the "stripe" phase (Fig. 2d) at $\gamma = -3$ ($\lambda_{di} = -15$). The bubble and stripe phases both consist of alternating 'up' and 'down' domains with a continuous variation of the dipolar orientation, and only differ in the shape of the domains. Neither of these phases has a global polarization ($P_1 \to 0$ in the thermodynamic limit), but due to their geometric difference they have either slight global in-plane (bubble, $Q_{zz} < 0$) or out-of-plane (stripe, $Q_{zz} > 0$) characteristics.

We construct the phase diagram of this system as λ_{dd}–λ_{di} sections for different fixed α (Fig. 3; see Supplementary Material for an alternative representation of the phase diagram). In addition to the four ordered phases identified above (IF, OAF, bubble, stripe) we find a disordered phase at low λ_{dd}, $|\lambda_{di}|$. When dipolar couplings dominate, we observe the IF phase, which transitions to either the OAF phase or the stripe phase upon increase of $|\lambda_{di}|$, when polarization interactions become dominant. For larger geometric ratio α (Fig. 3a) the IF phase transitions to the stripe phase via a narrow region exhibiting the bubble phase. This intermediate phase can be interpreted by noting that as $|\lambda_{di}|$ increases, the stripe phase forms via merging of circular domains (Fig. 2, between panels c and d), thereby reducing the area of the boundaries between oppositely oriented bubbles and thus the fraction of in-plane dipoles. As α is increased further, the stripe region grows at the expense of the IF and bubble regions (Fig. 3b). Conversely, for small α (Fig. 3c,d) the IF and disordered phases occupy larger regions of the

phase diagram, and the OAF phase replaces the stripe phase. Interestingly, when the competing parameters λ_{dd} and $|\lambda_{di}|$ become large enough to overwhelm entropic effects, at fixed α only their ratio determines the phase of the system (cf. diagonal phase boundaries in Fig. 3a,c,d).

What is then the role of the geometric factor α in the phase diagram of Fig. 3? We focus on conditions with strong polarization effects (large $|\lambda_{di}|$), where the dipoles are predominantly oriented out-of-plane. In addition to the first-order D–D and D–I interactions characterized by λ_{dd} and λ_{di}, respectively, dipoles interact with the surface polarization induced by *other* dipoles. The second-order D–I interaction (between a dipole and its nearest-neighbor images) is controlled by $\lambda_{di}^{(2)} = \lambda_{di}[\alpha^2/(1+\alpha^2)]^{3/2}$ and grows in magnitude with increasing α, at fixed λ_{di}. For large α, its contribution to the total energy becomes comparable to the first-order (direct) D–I interaction. Interestingly, precisely in this situation of large α, the secondary images promote the parallel alignment of neighboring dipoles (cf. dipolar field in Fig. 4a, left-hand side), opposing (and overwhelming) the influence of the direct D–D interaction between nearest neighbors. Thus, the second-order D–I interaction acts as an 'exchange parameter' with magnitude $|D_0| = |\frac{2\alpha^2-1}{\alpha^2+1}\lambda_{di}^{(2)}|$ that promotes short-range ferroelectric order (see Supplementary Material for derivation). However, at larger distances the dipolar coupling dominates and favors anti-ferroelectric order, resulting in modulated (i.e., stripe and bubble) phases. By contrast, at small α the 'exchange parameter' D_0 is not only smaller in magnitude, but owing to the geometry of the dipolar field it also favors the same anti-parallel alignment as imposed by the D–D interactions (Fig. 4a, right-hand side, see Supplementary Material for details). This explains why different values of α result in modulated (stripe) or nonmodulated (OAF) equilibrium phases at large $|\lambda_{di}|$.

The stripe phase, in particular, has been the subject of considerable attention [9, 13, 14, 45], notably its formation mechanism in different systems and the degree to which it can be controlled. Remarkably, the dielectric modulation mechanism identified here allows fine control over the stripe width $\tilde{w}$ via the geometric factor α. The reduced stripe width is defined as $\tilde{w} = \langle N/N_p \rangle$, where $N_p = \sum_{\langle jk \rangle} H(-\mu_{j,z}\mu_{k,z})$ is the number of dipole pairs at stripe interfaces selected by the Heaviside function $H(x) = [1 + \text{sgn}(x)]/2$. For fixed dipolar coupling λ_{dd} and dielectric coupling λ_{di}, the width of stripes can be manipulated accurately through variation of the geometric factor, as illustrated in Fig. 4b via $\tilde{w}$ as a function of α and D_0, as well as accompanying representative snapshots. The stripe width accurately reflects an exponential dependence on D_0 for sufficiently large $\tilde{w}$ (Fig. 4b), in accordance with predictions based upon the asymptotic expression for the ground-state energy of a 2D Ising dipole system [13]. Moreover, the domain-wall thickness t, which is determined by the balance between the exchange interaction D_0 and the surface anisotropy λ_{di}, increases with α. This is consistent with the theoretical prediction [46] that t scales as the square root of the ratio between the exchange enery and surface anisotropy.

In conclusion, we have demonstrated that dielectric effects can induce modulated phases in quasi-2D dipolar systems, without the presence of an additional competing interaction. Notably, the so-called striped and bubble patterns can be realized in dipolar films on a substrate with negative static permittivity and/or permeability. Accurate control of the properties of these modulated phases is possible via a geometric factor, related to particle shape and separation, which can be interpreted in terms of an effective 'exchange parameter' promoting local ferroelectricity. Besides elucidating the pattern-modulation mechanism, our findings may also provide guidance to future applications of such metamaterials.

---

[*] Corresponding author: luijten@northwestern.edu

[1] M. Seul and D. Andelman, "Domain shapes and patterns: The phenomenology of modulated phases," Science **267**, 476–483 (1995).

[2] D. Andelman and R. E. Rosensweig, "Modulated phases: Review and recent results," J. Phys. Chem. B **113**, 3785–3798 (2009).

[3] R. Allenspach, M. Stampanoni, and A. Bischof, "Magnetic domains in thin epitaxial Co/Au(111) films," Phys. Rev. Lett. **65**, 3344–3347 (1990).

[4] I. Booth, A. B. MacIsaac, J. P. Whitehead, and K. De'Bell, "Domain structures in ultrathin magnetic films," Phys. Rev. Lett. **75**, 950–953 (1995).

[5] K. De'Bell, A. B. MacIsaac, and J. P. Whitehead, "Dipolar effects in magnetic thin films and quasi-two-dimensional systems," Rev. Mod. Phys. **72**, 225–257 (2000).

[6] H. Möhwald, "Direct characterization of monolayers at the air–water interface," Thin Solid Films **159**, 1–15 (1988).

[7] D. Andelman, F. Broçhard, and J.-F. Joanny, "Phase transitions in Langmuir monolayers of polar molecules," J. Chem. Phys. **86**, 3673–3681 (1987).

[8] L. Leibler, "Theory of microphase separation in block copolymers," Macromolecules **13**, 1602–1617 (1980).

[9] M. P. Stoykovich, M. Müller, S. O. Kim, H. H. Solak, E. W. Edwards, J. J. de Pablo, and P. F. Nealey, "Di-
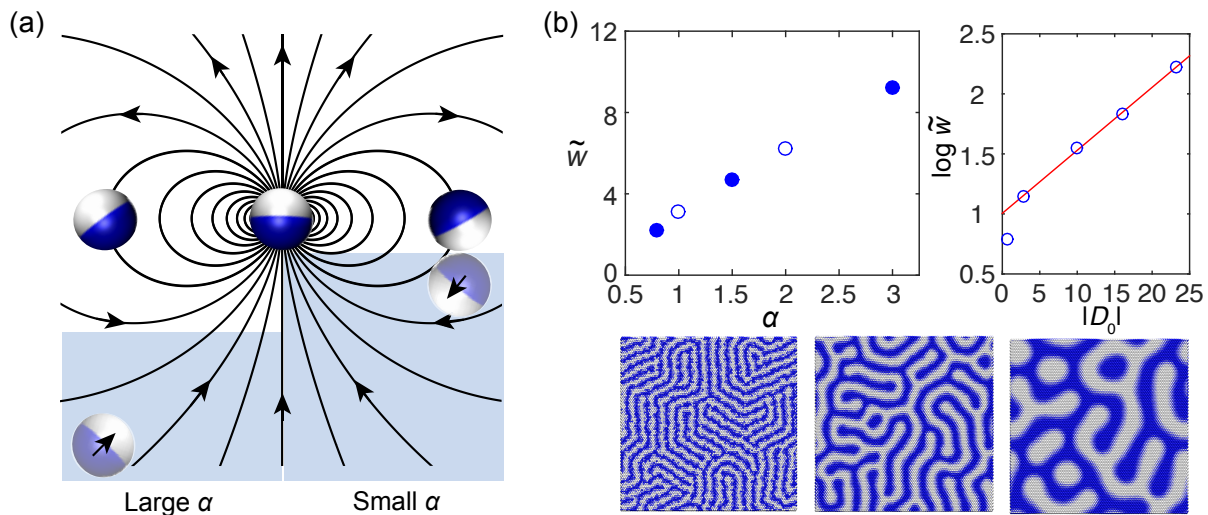
FIG. 4. (a) Role of geometric factor α in the effect of polarization charge on the (anti-)parallel alignment of neighboring dipolar particles. The schematic shows the electric field generated by a central dipole above a substrate (blue shaded region). The interaction with the "image" of a neighboring dipole (also shown) is characterized by the parameter $\lambda_{\mathrm{di}}^{(2)}$. At small geometric factor α (right) the field will promote anti-parallel alignment of the neighboring image dipole and hence also of the real dipole, in accordance with the direct dipole–dipole interaction. However, for large α (left), the polarization will promote parallel alignment of two neighboring dipoles, opposing the direct dipolar interaction. (b) Control of stripe width via the geometric factor. Reduced stripe width $\tilde{w}$ is shown as a function of α for fixed $\lambda_{\mathrm{dd}} = 5$ and $\lambda_{\mathrm{di}} = -16$ (upper left panel). The width exhibits an exponential dependence on the exchange parameter D_0 (upper right panel), confirming theoretical predictions. Representative equilibrium configurations of a 100×114 system are shown for $\alpha = 0.8$, 1.5, and 3 (lower panel).

rected assembly of block copolymer blends into nonregular device-oriented structures," Science **308**, 1442–1446 (2005).

[10] Y. A. Vlasov, X.-Z. Bo, J. C. Sturm, and D. J. Norris, "On-chip natural assembly of silicon photonic bandgap crystals," Nature **414**, 289–293 (2001).

[11] E. F. Borra, A. M. Ritcey, R. Bergamasco, P. Laird, J. Gingras, M. Dallaire, L. Da Silva, and H. Yockell-Lelievre, "Nanoengineered astronomical optics," Astron. Astrophys. **419**, 777–782 (2004).

[12] C. L. Dennis, R. P. Borges, L. D. Buda, U. Ebels, J. F. Gregg, M. Hehn, E. Jouguelet, K. Ounadjela, I. Petej, I. L. Prejbeanu, and M. J. Thornton, "The defining length scales of mesomagnetism: a review," J. Phys.: Condens. Matter **14**, R1175–R1262 (2002).

[13] A. B. MacIsaac, J. P. Whitehead, M. C. Robinson, and K. De'Bell, "Striped phases in two-dimensional dipolar ferromagnets," Phys. Rev. B **51**, 16033–16045 (1995).

[14] A. D. Stoycheva and S. J. Singer, "Stripe melting in a two-dimensional system with competing interactions," Phys. Rev. Lett. **84**, 4657–4660 (2000).

[15] A. B. MacIsaac, J. P. Whitehead, K. De'Bell, and P. H. Poole, "Phase diagram for a magnetic thin film with dipolar interactions and magnetic surface anisotropy," Phys. Rev. Lett. **77**, 739–742 (1996).

[16] K. D. Usadel and A. Hucht, "Anisotropy of ultrathin ferromagnetic films and the spin reorientation transition," Phys. Rev. B **66**, 024419 (2002).

[17] N. Osterman, D. Babič, I. Poberaj, J. Dobnikar, and P. Ziherl, "Observation of condensed phases of quasiplanar core-softened colloids," Phys. Rev. Lett. **99**, 248301 (2007).

[18] T. Garel and S. Doniach, "Phase transitions with spontaneous modulation – the dipolar Ising ferromagnet," Phys. Rev. B **26**, 325–329 (1982).

[19] J. Dobnikar, A. Snezhko, and A. Yethiraj, "Emergent colloidal dynamics in electromagnetic fields," Soft Matt. **9**, 3693–3704 (2013).

[20] V. Russier, "Calculated magnetic properties of two-dimensional arrays of nanoparticles at vanishing temperature," J. Appl. Phys. **89**, 1287–1294 (2001).

[21] J. J. Weis, J. M. Tavares, and M. M. Telo da Gama, "Structural and conformational properties of a quasi-two-dimensional dipolar fluid," J. Phys.: Condens. Matter **14**, 9171–9186 (2002).

[22] J.-J. Weis, "Simulation of quasi-two-dimensional dipolar systems," J. Phys.: Condens. Matter **15**, S1471–S1495 (2003).

[23] P. D. Duncan and P. J. Camp, "Structure and dynamics in a monolayer of dipolar spheres," J. Chem. Phys. **121**, 11322–11331 (2004).

[24] H. Schmidle, C. K. Hall, O. D. Velev, and S. H. L. Klapp, "Phase diagram of two-dimensional systems of dipole-like colloids," Soft Matt. **8**, 1521–1531 (2012).

[25] S. H. L. Klapp, "Monte-Carlo simulations of strongly interacting dipolar fluids between two conducting walls," Mol. Simul. **32**, 609–621 (2006).

[26] K. Takae and A. Onuki, "Applying electric field to charged and polar particles between metallic plates: Extension of the Ewald method," J. Chem. Phys. **139**, 124108 (2013).

[27] M. W. Knight, Y. Wu, J. B. Lassiter, P. Nordlander, and N. J. Halas, "Substrates matter: Influence of an adjacent dielectric on an individual plasmonic nanoparticle," Nano

Letters **9**, 2188–2192 (2009).

[28] H. S. Antila and E. Luijten, "Dielectric modulation of ion transport near interfaces," Phys. Rev. Lett. **120**, 135501 (2018).

[29] V. G. Veselago, "The electrodynamics of substances with simultaneously negative values of ε and μ," Sov. Phys. Usp. **10**, 509–514 (1968).

[30] D. R. Smith, J. B. Pendry, and M. C. Wiltshire, "Metamaterials and negative refractive index," Science **305**, 788–792 (2004).

[31] Y. Urzhumov, W. Chen, C. Bingham, W. Padilla, and D. R. Smith, "Magnetic levitation of metamaterial bodies enhanced with magnetostatic surface resonances," Phys. Rev. B **85**, 054430 (2012).

[32] M. W. Coffey, "Magnetic levitation from negative permeability materials," Phys. Lett. A **376**, 2739–2742 (2012).

[33] P. Hammond, "Electric and magnetic images," Proc. IEE - Part C **107**, 306–313 (1960).

[34] L. Hong, A. Cacciuto, E. Luijten, and S. Granick, "Clusters of charged Janus spheres," Nano Letters **6**, 2510–2514 (2006).

[35] O. V. Dolgov, D. A. Kirzhnits, and V. V. Losyakov, "On the admissible values of the static magnetic permeability," Solid State Commun. **46**, 147–149 (1983).

[36] J. B. Kana Kana, G. Vignaud, A. Gibaud, and M. Maaza, "Thermally driven sign switch of static dielectric constant of vo2 thin film," Opt. Mater. (Amst) **54**, 165–169 (2016).

[37] V. U. Nazarov, "Negative static permittivity and violation of Kramers-Kronig relations in quasi-two-dimensional crystals," Phys. Rev. B **92**, 161402(R) (2015).

[38] C. W. Chu, F. Chen, J. Shulman, S. Tsui, Y. Y. Xue, W. Wen, and P. Sheng, "A negative dielectric constant in nano-particle materials under an electric field at very low frequencies," Strongly Correl. Electron Mater. Phys. Nanoeng. **5932**, 59320X (2006).

[39] J. Shulman, S. Tsui, F. Chen, Y. Y. Xue, and C. W. Chu, "Plasmalike negative capacitance in nanocolloids," Appl. Phys. Lett. **90**, 8–11 (2007).

[40] H. Yan, C. Zhao, K. Wang, L. Deng, M. Ma, and G. Xu, "Negative dielectric constant manifested by static electricity," Appl. Phys. Lett. **102**, 062904 (2013).

[41] R. Mach-Batlle, A. Parra, J. Prat-Camps, S. Laut, C. Navau, and A. Sanchez, "Negative permeability in magnetostatics and its experimental demonstration," Phys. Rev. B **96**, 094422 (2017).

[42] Z. Wang and E. Luijten, "Structural and dynamical properties of dipolar fluids near a dielectric interface," (2019), in preparation.

[43] M. P. Allen and D. J. Tildesley, *Computer Simulation of Liquids* (Clarendon, Oxford, 1987).

[44] A. van Blaaderen, R. Ruel, and P. Wiltzius, "Template-directed colloidal crystallization," Nature **385**, 321–324 (1997).

[45] G. Malescio and G. Pellicane, "Stripe phases from isotropic repulsive interactions," Nature Mater. **2**, 97–100 (2003).

[46] R. C. O'Handley, *Modern Magnetic Materials: Principles and Applications* (Wiley, New York, 1999).